Effects of Water Dissociation and CO_2 Contamination on the Electrophoretic Mobility of a Spherical Particle in Aqueous Salt-Free Concentrated Suspensions

Félix Carrique*,† and Emilio Ruiz-Reina‡

Departamento de Física Aplicada I, Campus de Teatinos, and Departamento de Física Aplicada II, Campus de El Ejido, Universidad de Málaga, 29071, Málaga, Spain

Received: February 20, 2009; Revised Manuscript Received: April 22, 2009

In a very recent paper (Ruiz-Reina, E.; Carrique, F. *J. Phys. Chem. B* **2008**, *112*, 11960.) we studied the effect of water dissociation and CO_2 contamination on the equilibrium electrical double layer of spherical particles in salt-free concentrated suspensions in aqueous solutions. It was shown that in most cases (dilute to moderately concentrated suspensions), the neglecting of those effects would lead to a very poor description of common salt-free suspensions, especially if the suspensions have been in contact with air. In the present contribution we explore the influence of the latter effects on the dc electrophoresis in realistic salt-free suspensions. This kind of system consists of aqueous suspensions without any electrolyte added during the preparation. The ionic species in solution can solely be (i) the "added counterions" stemming from the particles that counterbalance their surface charge, (ii) the H^+ and OH^- ions from water dissociation, and (iii) the ions produced by the atmospheric CO_2 contamination. Our model follows the classical Poisson−Boltzmann approach, a spherical cell model and the appropriate local chemical reactions. We have applied it to the study of the electrophoretic mobility of a spherical particle for different particle volume fractions ϕ and surface charge densities. The numerical results have shown the quite large influence that water dissociation ions and/or CO_2 contamination have on the electrophoretic mobility at low-moderate particle volume fractions. In those situations the role of the added counterions is screened by the other ionic species. These effects yield the mobility to reach plateau values instead of further increasing as volume fraction decreases. It is concluded that it is necessary to take into account the water dissociation influence for ϕ lower than approximately 10^{-2}, whereas the atmospheric contamination, if the suspensions have been exposed to the atmosphere, is not negligible if $\phi < 10^{-1}$. The present work sets the basis for further theoretical models concerning particularly the ac electrokinetics and dielectric response of such systems.

Introduction

An increasing interest is nowadays being dedicated to the study of salt-free colloidal suspensions.[1−13] The term salt-free does not mean that there are not ions present in the suspension because those ions stemming from the charging process of the colloidal particles, which are known as "added counterions", surround the particle preserving the electroneutrality. Well-known features of these salt-free suspensions include, for example, a singular relationship between the surface potential and the surface charge density,[3,4] the phenomenon of the counterion condensation,[3,4,9] surprising shifts to larger frequencies of the Maxwell−Wagner−O'Konski relaxation process,[12,13] and its effect on the dynamic electrophoretic mobility, etc. Another important aspect concerns the distinction between actual particle charge (bare charge) and renormalized charge,[14] as commonly used when interpreting electrokinetics and interactions between charged colloidal particles.

The study of the ionic condensation effect by using a cell model concept was already explored in the 1980s by Alexander.[14] More recently,[15−18] it has also been analyzed by numerical simulations[19] and extended with the inclusion of chemical surface reactions for the generation of the particle charge.[19] The present treatment incorporates realistic chemistry to exhaustively deionized concentrated suspensions (they will be called realistic salt-free suspensions hereafter), although surface group dissociation studies, as that by Palberg et al.,[20] will not be addressed in this work.

In analogy with the case of suspensions in salt solutions, a Debye length κ^{-1} characterizing the width of the electrical double layer in a pure salt-free suspension, has been recently defined:[21]

$$\kappa^2 = \frac{e^2 \bar{n}_c z_c^{\,2}}{\varepsilon_0 \varepsilon_{rs} k_B T} = \frac{-3 e z_c}{\varepsilon_0 \varepsilon_{rs} k_B T a} \sigma \frac{\phi}{1-\phi} \qquad (1)$$

where e is the elementary electric charge, k_B is the Boltzmann constant, T is the absolute temperature, ε_{rs} is the relative permittivity of the suspending medium, ε_0 is the vacuum permittivity, a is the particle radius, σ is the particle surface charge density, ϕ is the volume fraction of particles, and $\bar{n}_c$ and z_c are the mean number density in the liquid medium and the valence of the added counterions. In the final section prior to the conclusions, a new definition of κ^{-1} will be presented because of the inconsistencies of eq 1 at very low particle volume fraction and surface charge. The new one is intended to represent the ionic screening effect of the particle, but unfortunately it requires complicated numerical computations. We will return to this issue at the end of the paper.

In a previous work concerning the equilibrium double layer (EDL) of a spherical particle in a realistic aqueous salt-free

* To whom correspondence should be addressed. E-mail: carrique@uma.es.
† Departamento de Física Aplicada I.
‡ Departamento de Física Aplicada II.

10.1021/jp9015905 CCC: $40.75
Published on Web 06/01/2009

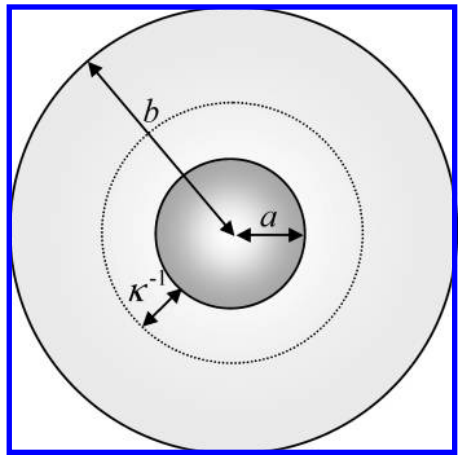

Figure 1. Cell model.

concentrated suspension,[11] it was stated that the roles of water dissociation ions and those coming from CO_2 contamination were crucial to model a realistic EDL. This is an important issue because there does not exist any aqueous salt-free suspension fully deionized of species, different, of course, of its added counterions. At least, the H^+ and OH^- ions from water dissociation will always be present in it accompanying the added counterions released by the particles.

In this work we study the electrophoretic mobility for the cases whose EDLs were described in ref 11, concerning (i) the only presence of added counterions, (ii) the inclusion of H^+ and OH^- ions from water dissociation, and (iii) the ions originated by the atmospheric CO_2 contamination. For all these cases, we have studied the influence of the surface charge density and the particle volume fraction on the dc electrophoretic mobility. Thus, in the following sections we describe the spherical cell model approach used in our model and the theoretical electrophoretic mobility predictions for the cases of pure and realistic salt-free suspensions, in order to quantify the new effects in comparison with the standard predictions.

Theory

Cell Model. In order to take into account the overlapping of adjacent electric double layers a cell model is used. The cell model concept has been successfully applied to develop theoretical models for different electrokinetic phenomena in moderately concentrated colloidal suspensions of charged particles, such as static electrophoresis and electrical conductivity,[22−25] sedimentation velocity and potential,[26,27] dynamic electrophoresis,[12,28−30] complex conductivity and dielectric response,[13,31] electroviscous effect[32−34] and electroacoustic phenomena,[35,36] to mention just a few. An excellent review on the use of the spherical cell approach has been recently written by Zholkovskij et al.[37]

According to this model (Figure 1), each spherical particle of radius a is surrounded by a concentric shell of the liquid medium, having an outer radius b such that the particle/cell volume ratio in the cell is equal to the particle volume fraction throughout the entire suspension,[38,39] i.e.,

$$\phi = \left(\frac{a}{b}\right)^3 \tag{2}$$

The basic assumption of the cell model is that the suspension properties can be derived from the study of a unique cell. By its own nature, the cell model is only applicable when the suspension is homogeneous and isotropic.

Electrokinetic Equations and Boundary Conditions. Let us consider that the charged spherical particle bears a surface charge density σ, and it is immersed in an aqueous solution of relative permittivity ε_{rs} and viscosity η_s, containing added counterions of valence z_c and drag coefficient λ_c, which stem from the charge generation process on the particles, as well as other, for the moment, unspecified ionic species. We will henceforth represent the ionic species with an index j ($j = 1, ..., n$), with valence z_j and drag coefficient λ_j, being the added counterion species associated to the value $j = 1$, i.e., $z_1 = z_c$ and $\lambda_1 = \lambda_c$. The amount of added counterions in solution exactly counterbalances the charge on the particles. In the presence of a static electric field $\mathbf{E}$ the particle moves with a uniform velocity $\mathbf{v}_e$, the electrophoretic velocity. The axes of a spherical coordinate system (r, θ, φ) are fixed at the center of the particle, with the polar axis ($\theta = 0$) parallel to the electric field. The solution of the problem requires us to know, at every point $\mathbf{r}$ of the system, relevant quantities such as the electrical potential $\Psi(\mathbf{r})$, the number density of ions $n_j(\mathbf{r})$ ($j = 1, ..., n$), their drift velocity $\mathbf{v}_j(\mathbf{r})$ ($j = 1, ..., n$), the fluid velocity $\mathbf{v}(\mathbf{r})$, and the pressure $p(\mathbf{r})$. The fundamental equations connecting them are well-known:[28,40−42]

$$\nabla^2\Psi(\mathbf{r}) = -\frac{\rho_{el}(\mathbf{r})}{\varepsilon_{rs}\varepsilon_0} \tag{3}$$

$$\rho_{el}(\mathbf{r}) = \sum_{j=1}^{n} z_j e n_j(\mathbf{r}) \tag{4}$$

$$\eta_s\nabla^2\mathbf{v}(\mathbf{r}) - \nabla p(\mathbf{r}) - \rho_{el}(\mathbf{r})\nabla\Psi(\mathbf{r}) = 0 \tag{5}$$

$$\nabla\cdot\mathbf{v}(\mathbf{r}) = 0 \tag{6}$$

$$\mathbf{v}_j(\mathbf{r}) = \mathbf{v}(\mathbf{r}) - \frac{1}{\lambda_j}\nabla\mu_j(\mathbf{r}) \qquad (j = 1, ..., n) \tag{7}$$

$$\mu_j(\mathbf{r}) = \mu_j^\infty + z_j e\Psi(\mathbf{r}) + k_B T \ln n_j(\mathbf{r}) \qquad (j = 1, ..., n) \tag{8}$$

$$\nabla\cdot[\sum_{j=1}^{N} z_j e n_j(\mathbf{r})\mathbf{v}_j(\mathbf{r})] = 0 \tag{9}$$

$$\nabla\cdot[n_c(\mathbf{r})\mathbf{v}_c(\mathbf{r})] = 0 \tag{9′}$$

where $\mu_j(\mathbf{r})$ is the chemical potential of the jth ionic species, with μ_j^∞ its standard value. Equation 3 is Poisson's equation, where $\rho_{el}(\mathbf{r})$ is the electric charge density given by eq 4. Equations 5 and 6 are the Navier−Stokes equations appropriate to a steady incompressible fluid flow at low Reynolds number in the presence of an electrical body force. Equation 7 mean that the ionic flow is provoked by the liquid flow and the gradient of the electrochemical potential defined in eq 8, and it is related to the Nernst−Planck equations for ionic fluxes. The drag coefficient λ_j in eq 7 is related to the limiting ionic conductance Λ_j^0 by[40]

$$\lambda_j = \frac{N_A e^2 |z_j|}{\Lambda_j^0} \qquad (j = 1, ..., n) \tag{10}$$

where N_A is Avogadro's number. It is worth mentioning that the continuity eq 9 stands for charge conservation instead of conservation of the number of every ionic species in the system. Besides, we are admitting that the possible chemical reactions that take place in the system are faster than any other ionic processes in response to the applied constant electric field, to ensure chemical local equilibrium in every point of the suspensions. As now we have just one charge continuity equation instead of the usual n ionic equations when no chemical reactions are present, we need $n - 1$ more equations to completely solve the problem. For that purpose, and as a first approximation, an equilibrium scheme for chemical reactions will be followed and their mass-action equations used locally in addition to the latter general system of eqs 3−9. In the particular case the added counterions were of a different ionic species as those associated with water dissociation and CO_2 contamination, and therefore, its concentration not linked with the other ones by chemical reactions, we can use a continuity equation for the conservation of the number of just the added counterions (eq 9′), in addition to the general continuity equation for the charge conservation (eq 9). In that case we still need $n - 2$ more equations to solve the problem than can be obtained from the chemical equilibrium reactions related to the ions different from the added counterions.

It is useful to apply a perturbation scheme as follows:

$$n_j(\mathbf{r}) = n_j^{(0)}(r) + \delta n_j(\mathbf{r}) \qquad (j = 1, ..., n)$$

$$\Psi(\mathbf{r}) = \Psi^{(0)}(r) + \delta\Psi(\mathbf{r}) \tag{11}$$

$$\mu_j(\mathbf{r}) = \mu_j^{(0)} + \delta\mu_j(\mathbf{r}) \qquad (j = 1, ..., n)$$

where quantities with superscript "(0)" refer to equilibrium values, and for low applied field strengths the perturbations will be considered linearly dependent on the field, and second and higher orders are dropped. Thus, neglecting any nonlinear perturbation term, we may write

$$\delta\mu_j = z_j e\delta\Psi + k_B T \delta n_j / n_j^{(0)} \qquad (j = 1, ..., n) \tag{12}$$

where the equilibrium volume charge density is given by

$$\rho_{el}^{(0)}(r) = \sum_{j=1}^{n} z_j e n_j^{(0)}(r) \tag{13}$$

and the equilibrium ionic concentration

$$n_j^{(0)}(r) = b_j \exp\left(-\frac{z_j e\Psi^{(0)}(r)}{k_B T}\right) \qquad (j = 1, ..., n) \tag{14}$$

obeys the Boltzmann distribution. The still unknown prefactors b_j ($j = 1, ..., n$) represent the concentration of ions at a point where the electrical potential is set to zero that, for numerical convenience, we have chosen at the outer surface of the cell

$$\Psi^{(0)}(b) = 0 \tag{15}$$

For the special case of just one ionic species, the added counterions ($j = 1$ case), the following condition must be fulfilled for electroneutrality reasons:

$$\int_a^b n_c^{(0)}(r) 4\pi r^2 \, dr = \int_a^b b_c \exp\left(-\frac{z_c e\Psi^{(0)}(r)}{k_B T}\right) 4\pi r^2 \, dr$$

$$= \frac{-4\pi a^2 \sigma}{z_c e} \tag{16}$$

In this case, the coupling between the particle surface charge and the total amount of added counterions released from each particle to the solution leads to an integro−differential Poisson−Boltzmann equation

$$\frac{1}{r^2}\frac{d}{dr}\left(r^2 \frac{d\Psi^{(0)}}{dr}\right) = -\frac{1}{\varepsilon_{rs}\varepsilon_0} z_c e n_c^{(0)}(r) \tag{17}$$

with

$$n_c^{(0)}(r) = \frac{(-4\pi a^2 \sigma) \exp\left(-\frac{z_c e\Psi^{(0)}(r)}{k_B T}\right)}{z_c e \int_a^b \exp\left(-\frac{z_c e\Psi^{(0)}(r)}{k_B T}\right) 4\pi r^2 \, dr} \tag{18}$$

and the boundary conditions are expressed by eq 16 and

$$\frac{d\Psi^{(0)}}{dr}(b) = 0 \tag{19}$$

or, alternatively, by the latter eq 19 and

$$\frac{d\Psi^{(0)}}{dr}(a) = -\frac{\sigma}{\varepsilon_{rs}\varepsilon_0} \tag{20}$$

coming from the electroneutrality of the cell and Gauss theorem. It is important to point out that the eq 16 is equivalent to eq 20, because by integrating eq 17 from a to b, and by using eqs 18 and 19, we obtain eq 20. Returning to the general case, we have more ionic species apart from those of the added counterions. In such conditions we will have to modify some of the latter boundary conditions, not only to obviously include all the ionic species, but also to take into account whether the added counterions are coincident or not with one of the other ionic species in the system. Those cases will be properly analyzed in further sections.

For the rest of fundamental equations the boundary conditions are

$$\Psi_p(\mathbf{r}) = \Psi(\mathbf{r}) \qquad \text{at} \quad r = a \tag{21}$$

$$\varepsilon_{rs}\nabla\Psi(\mathbf{r})\cdot\hat{\mathbf{r}} - \varepsilon_{rp}\nabla\Psi_p(\mathbf{r})\cdot\hat{\mathbf{r}} = -\sigma/\varepsilon_0 \qquad \text{at} \quad r = a \tag{22}$$

$$\mathbf{v} = 0 \qquad \text{at} \quad r = a \tag{23}$$

$$\mathbf{v}_j\cdot\hat{\mathbf{r}} = 0 \qquad \text{at} \quad r = a \qquad (j = 1, ..., n) \tag{24}$$

$$v_r = -\mathbf{v}_e\cdot\hat{\mathbf{r}} \qquad \text{at} \quad r = b \tag{25}$$

$$\boldsymbol{\omega} = \nabla\times\mathbf{v} = 0 \qquad \text{at} \quad r = b \tag{26}$$

where $\Psi_p(\mathbf{r})$ is the electrical potential in the interior region of the solid particle and ε_{rp} its relative permittivity.

Equation 21 expresses the continuity of the electrical potential at the surface of the particle. Equation 22 relates the discontinuity of the normal component of the electrical displacement vector with the particle charge density, where $\hat{\mathbf{r}}$ is the normal vector outward to the surface. Equation 23 means that the liquid cannot slip on the particle. Additionally, and due to the nonconducting nature of the particle, the velocity of ions in the normal direction to the particle surface is zero, as represented by eq 24. In the outer surface of the cell ($r = b$), we will follow Kuwabara's boundary conditions. In the radial direction, the velocity of the liquid will be minus the radial component of the electrophoretic velocity, as expressed by eq 25, and finally, eq 26 means that the liquid flow is free of vorticity on that surface.

As indicated before, it is convenient to write the nonequilibrium quantities in terms of their equilibrium values plus a field-dependent perturbation. Substituting into the differential equations the above-mentioned perturbation scheme, neglecting products of small perturbation quantities, and making use of the symmetry conditions of the problem[4]

$$\mathbf{v}(\mathbf{r}) = (v_r, v_\theta, v_\varphi) = \left(-\frac{2}{r}hE\cos\theta, \frac{1}{r}\frac{d}{dr}(rh)E\sin\theta, 0\right) \tag{27}$$

$$\delta\mu_j(\mathbf{r}) = -z_j e\phi_j(r)E\cos\theta \qquad (j = 1, ..., n) \tag{28}$$

$$\delta\Psi = -Y(r)E\cos\theta \tag{29}$$

we obtain

$$L(Lh) = -\frac{e^2}{\eta_s k_B T r}\left(\frac{d\Psi^{(0)}}{dr}\right)\sum_{j=1}^{n} z_j^2 n_j^{(0)}(r)\phi_j(r) \tag{30}$$

$$\sum_{j=1}^{n}\frac{z_j^2 e^2 n_j^{(0)}(r)}{\lambda_j}\left\{L\phi_j(r) - \frac{e}{k_B T}\left(\frac{d\Psi^{(0)}}{dr}\right)\left(z_j\frac{d\phi_j}{dr} - \frac{2\lambda_j}{e}\frac{h(r)}{r}\right)\right\} = 0 \tag{31}$$

$$L\phi_c(r) = \frac{e}{k_B T}\left(\frac{d\Psi^{(0)}}{dr}\right)\left(z_c\frac{d\phi_c}{dr} - \frac{2\lambda_c}{e}\frac{h(r)}{r}\right) \tag{31'}$$

$$LY(r) = \frac{e^2}{\varepsilon_{rs}\varepsilon_0 k_B T}\sum_{j=1}^{n} z_j^2 n_j^{(0)}(r)[Y(r) - \phi_j(r)] \tag{32}$$

where the L operator is defined by

$$L \equiv \frac{d^2}{dr^2} + \frac{2}{r}\frac{d}{dr} - \frac{2}{r^2} \tag{33}$$

and eq 31′ corresponds to the case the added counterions be of a different ionic species as the rest of ions in solution.

In terms of perturbed quantities, the electrochemical potential of ions satisfies

$$\nabla\delta\mu_j\cdot\hat{\mathbf{r}} = 0|_{r=a} \qquad (j = 1, ..., n) \tag{34}$$

which follows by considering eqs 7, 11, 23, and 24. Furthermore and concerning the ionic perturbation at the outer surface of the cell, we choose the boundary condition:

$$\delta n_j(b) = 0 \qquad (j = 1, ..., n) \tag{35}$$

It was first introduced by Shilov et al.[44] and, since then, has been commonly used by many authors[25,29,31,45,46] in electrokinetic cell models.

Likewise, the electric perturbation at the particle surface becomes

$$\delta\Psi(\mathbf{r})|_{r=a} = \delta\Psi_p(\mathbf{r})|_{r=a} \tag{36}$$

$$\varepsilon_{rs}(\nabla\delta\Psi(\mathbf{r})\cdot\hat{\mathbf{r}})|_{r=a} = \varepsilon_{rp}(\nabla\delta\Psi_p(\mathbf{r})\cdot\hat{\mathbf{r}})|_{r=a} \tag{37}$$

where, analogously to eq 29, the inner electrical potential perturbation can be expressed as

$$\delta\Psi_p(\mathbf{r}) = -Y_p(r)E\cos\theta \tag{38}$$

According to symmetry considerations, the boundary conditions in eqs 23, 26, and 34−38 transform into

$$h(a) = \frac{dh}{dr}(a) = 0 \tag{39}$$

$$Lh(b) = 0 \tag{40}$$

$$\frac{d\phi_j}{dr}(a) = 0 \qquad (j = 1, ..., n) \tag{41}$$

$$\phi_j(b) = Y(b) \qquad (j = 1, ..., n) \tag{42}$$

$$\frac{dY}{dr}(a) - \frac{\varepsilon_{rp}}{\varepsilon_{rs}}\frac{Y(a)}{a} = 0 \tag{43}$$

In addition, we must impose the constraint that in the stationary state the net force acting on the particle or the unit cell must be zero. This condition can be expressed as[43]

$$\eta_s\frac{d}{dr}[rLh(r)]|_{r=b} - \rho_{el}^{(0)}(b)Y(b) = 0 \tag{44}$$

We also need boundary conditions at the outer surface of the cell for the perturbation quantities $\delta\Psi$ or $Y(r)$. Dukhin et al.[47] proposed a Dirichlet-type electrical boundary condition

according to the Shilov−Zharkikh−Borkovskaya cell model,[44] showing the connection between the macroscopic, experimentally measured electric field $\langle \mathbf{E} \rangle$ and local electrical properties

$$\delta\Psi(\mathbf{r})|_{r=b} = -Eb\cos\theta \tag{45}$$

where $E = |\langle \mathbf{E} \rangle|$, or in terms of the function $Y(r)$,

$$Y(b) = b \tag{46}$$

This electrical boundary condition has been applied by many authors in different electrokinetic cell models.[3,25,29,30,42,46] We use the mathematical application MATLAB with its built-in routines to numerically solve the full set of differential eqs 30−32 and boundary conditions in eqs 39−44, and 46. Previously, we have to solve the equilibrium Poisson−Boltzmann equation coupled with the equations for the ionic equilibrium chemical reactions, to allow the unknown concentration prefactors b_j ($j = 1, ..., n$) to be obtained. The boundary value problem solver used is a finite difference code that implements the three-stage Lobatto−Illa formula. This is a collocation formula and the collocation polynomial provides a C^1-continuous solution that is fourth-order accurate uniformly in the functions domain.[48] Mesh selection and error control are based on the residual of the continuous solution. The relative tolerance, which applies to all components of the residual vector, has been taken equal to 10^{-6}.

Electrophoretic Mobility

The electrophoretic mobility μ of a spherical particle in a concentrated colloidal suspension can be defined from the relation between the electrophoretic velocity of the particle $\mathbf{v}_e$ and the macroscopic electric field $\langle \mathbf{E} \rangle$. From the boundary eq 25: $v_r = -\mathbf{v}_e \cdot \hat{\mathbf{r}}$, at $r = b$, the definition $|\mathbf{v}_e| = \mu E$ (with $E = |\langle \mathbf{E} \rangle|$) and the symmetry eq 27, we obtain

$$\mu = \frac{2h(b)}{b} \tag{47}$$

In the past few years some models valid for pure salt-free electrophoresis have been derived. Ohshima derived one for low particle concentration and got analytical expressions for the electrophoretic mobility for either low or very high surface charges.[5,6] His main conclusions were that the electrophoretic mobility follows two distinct behaviors separated by a certain critical surface charge value. Below this critical point, the electrophoretic mobility satisfies a Hückel law linearly connecting electrophoretic mobility and particle charge. Because of the counterion condensation effect, for charges higher than the critical one the electrophoretic mobility reaches a plateau and becomes practically independent of particle charge. These results were recently confirmed by Chiang et al.,[3] and extended to arbitrary particle concentration. We also addressed the electrophoresis and conductivity of pure salt-free suspensions in a very recent contribution where different frames of boundary conditions, typically found in the literature, were explored.[9]

In what follows we will analyze the singularities the electrophoretic mobility shows in more "realistic" salt-free suspensions including either water dissociation or water dissociation plus CO_2 contamination, as compared with pure salt-free electrophoretic mobility predictions. As usual, the mobility data will be scaled as

$$\mu^* = \frac{3\eta_s e}{2\varepsilon_{rs}\varepsilon_0 k_B T}\mu \tag{48}$$

where μ^* is the nondimensional electrophoretic mobility. A first and crucial step before addressing that issue is to solve the equilibrium Poisson−Boltzmann equation for the cases we are concerned, because the equilibrium electrical potential $\Psi^{(0)}(r)$ explicitly appears in the differential electrokinetic equations. In the following sections and for clarity, brief introductions of the procedures used in every case will be shown. Interested readers can find a full description of the mathematical details in a recent contribution from the authors.[11]

Electrophoretic Mobility: Added Counterions and Water Dissociation. Let us consider now that, in addition to the added counterions stemming from the particle charging process, there are also H^+ and OH^- ions coming from water dissociation in the liquid medium. This will always occur in aqueous suspensions. We can distinguish between two cases: (a) when the added counterions are H^+ or OH^- ions (number of different ionic species $n = 2$) and (b) when they are all of a different ionic species ($n = 3$). The distinction is important because in the a case the added counterions will enter in the reaction equation for water dissociation, whereas in the b case they do not. We will use nondimensional variables, which are defined by

$$x = \frac{r}{a}, \quad \tilde{\Psi}^{(0)}(x) = \frac{e\Psi^{(0)}(r)}{k_B T}, \quad \tilde{b}_j = \frac{e^2 a^2}{\varepsilon_{rs}\varepsilon_0 k_B T} b_j \quad (j = 1, ..., n),$$
$$\tilde{\sigma} = \frac{ea}{\varepsilon_{rs}\varepsilon_0 k_B T}\sigma \tag{49}$$

Case a. In this case, the nondimensional Poisson−Boltzmann equation becomes[11]

$$\tilde{\Psi}'''(x) + \frac{2}{x}\tilde{\Psi}''(x) - \frac{2}{x^2}\tilde{\Psi}'(x) - \tilde{\Psi}'(x)\sqrt{\left(\tilde{\Psi}''(x) + \frac{2}{x}\tilde{\Psi}'(x)\right)^2 + 4\tilde{K}_w} = 0 \tag{50}$$

by using a novel and very efficient mathematical treatment developed by the authors in the same ref 11. This is a nonlinear third-order differential equation that needs three boundary conditions to completely specify the solution. They are provided by eqs 15, 19, and 20, that now read

$$\tilde{\Psi}^{(0)}(x = s) = 0 \qquad \tilde{\Psi}^{(0)\prime}(x = s) = 0 \qquad \tilde{\Psi}^{(0)\prime}(x = 1) = -\tilde{\sigma} \tag{51}$$

where $s = (b/a) = \phi^{-1/3}$. By taking the ionic valences $z_{H^+} = 1$ and $z_{OH^-} = -1$ and the equilibrium mass-action equation for water dissociation, which we assume to hold at any point in the liquid medium, we obtain

$$[H^+][OH^-] = K_w \Rightarrow \tilde{b}_{H^+}\tilde{b}_{OH^-} = \tilde{K}_w \tag{52}$$

where eqs 14 and 49 have been used. The square brackets in eq 52 stand for molar concentrations, $K_w = 10^{-14}$ mol^2/L^2 is the water dissociation constant at room temperature 298.16 K,

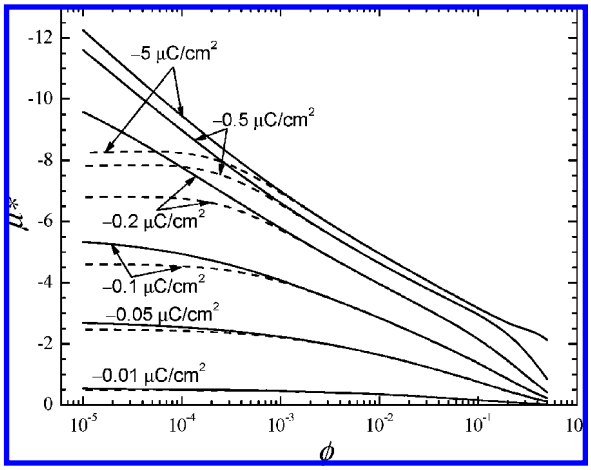

Figure 2. Nondimensional electrophoretic mobility against particle volume fraction for different surface charge densities. Solid lines: only added counterions H^+. Dashed lines, case a: added counterions H^+ with water dissociation ions H^+, OH^-.

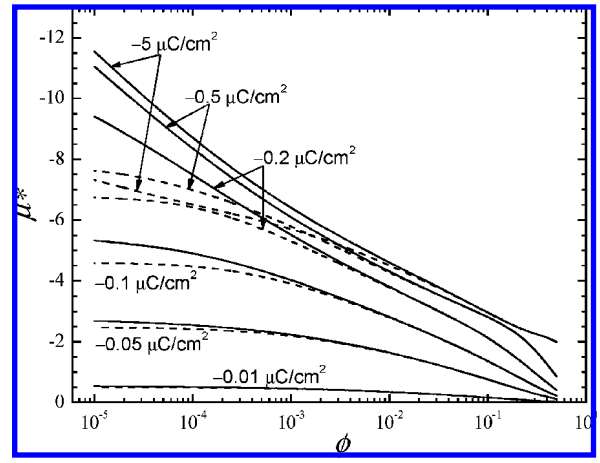

Figure 3. Nondimensional electrophoretic mobility against particle volume fraction for different surface charge densities. Solid lines: only added counterions K^+. Dashed lines, case b: added counterions K^+ with water dissociation ions H^+, OH^-.

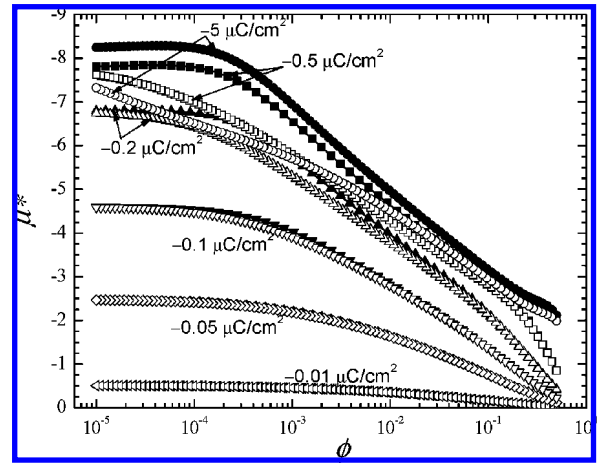

Figure 4. Nondimensional electrophoretic mobility against particle volume fraction for different surface charge densities and type of added counterions. Solid symbols, case a: added counterions H^+ with water dissociation ions H^+, OH^-. Open symbols, case b: added counterions K^+ with water dissociation ions H^+, OH^-.

and $\tilde{K}_w$ in eqs 50 and 52 is a nondimensional quantity defined by

$$\tilde{K}_w = \left(\frac{N_A e^2 a^2}{\varepsilon_{rs}\varepsilon_0 k_B T}\right)^2 K_w \tag{53}$$

all the values taken in SI units. The electroneutrality of the cell implies that

$$\tilde{\sigma} = -\tilde{b}_{H^+}\int_1^s x^2 e^{-\tilde{\Psi}^{(0)}(x)}\,dx + \tilde{b}_{OH^-}\int_1^s x^2 e^{\tilde{\Psi}^{(0)}(x)}\,dx \tag{54}$$

and sets the electrical state of the particle surface.

We can solve eq 50 numerically in one single step to obtain the equilibrium electric potential.[11]

Once we have found the electric potential $\tilde{\Psi}^{(0)}(x)$, the parameters $\tilde{b}_{H^+}$ and $\tilde{b}_{OH^-}$ can be obtained from the system of equations[11]

$$\tilde{b}_{H^+}\tilde{b}_{OH^-} = \tilde{K}_w, \quad \tilde{\Psi}^{(0)\prime\prime}(s) = -\tilde{b}_{H^+} + \tilde{b}_{OH^-} \tag{55}$$

and the equilibrium ionic concentrations can be calculated with the help of eq 14.

In all the theoretical Figures 2−12, the temperature T, the relative permittivity of the suspending liquid ε_{rs}, and the radius of the particles have been chosen as 298.16 K, 78.55, and 100 nm, respectively. In Figure 2 we show the effect of water dissociation ions on the electrophoretic mobility for the present case a in comparison with the prediction for a pure salt-free suspension with the same type of added counterions (H^+). It is well-known the monotonous decrease of the mobility as volume fraction increases in a pure salt-free suspension[9] due to the increasing number of neighbors and consequently the diminution of the particle diffusion length. But what is more noticeable is the presence of plateaus in mobility at low volume fractions when water dissociation effects are taking into account. The effect is relatively more important the larger the particle charge. Another interesting feature is that for highly concentrated suspensions there are no differences between curves corresponding to pure and realistic suspensions. This is due to the increase of the number of added counterions as volume fraction increases, tending to screen the effect of water dissociation ions. The opposite seems to occur at very low volume fractions. In this region the H^+ ions stemming from water dissociation dominate over those associated with the particle charging mechanism. In addition, the augmented concentration of counterions inside the cell in the latter conditions yields a better masking of the particle charge which also traduces in an important decrease of the surface potential, as already described in a previous work,[11] and therefore, on the electrophoretic mobility. On the other hand, it was reported that the mobility increases with the particle charge at a given volume fraction, from a roughly linear region at low charge values, to an almost independent value at sufficiently high particle charge (the so-called ionic condensation effect[3,5,6,9]). It is clear in Figure 2 how the mobility curves tend to approach each others at the larger particle charges. In any case what is worthwhile mentioning is the necessity at every particle charge of a certain particle volume fraction to overcome the effects of water dissociation ions. This point is crucial because in typical electrophoretic mobility determinations in dilute conditions, the expected ζ-potentials or electrokinetic particle charges that can be obtained from standard theories might be erroneous.

Case b. In this case, by applying the same mathematical treatment above referred,[11] the nondimensional Poisson−Boltzmann equation transforms to

$$\tilde{\Psi}^{(0)\prime\prime\prime}(x) + \frac{2}{x}\tilde{\Psi}^{(0)\prime\prime}(x) - \frac{2}{x^2}\tilde{\Psi}^{(0)\prime}(x) - \tilde{\Psi}^{(0)\prime}(x) \times \left[\sqrt{\left(\tilde{\Psi}^{(0)\prime\prime}(x) + \frac{2}{x}\tilde{\Psi}^{(0)\prime}(x) + z_c\tilde{b}_c e^{-z_c\tilde{\Psi}^{(0)}(x)}\right)^2 + 4\tilde{K}_w} + z_c^2\tilde{b}_c e^{-z_c\tilde{\Psi}^{(0)}(x)}\right] = 0 \quad (56)$$

where again we designate by the subindex "c" quantities relative to the added counterion species. The added counterions balance the overall charge on the particle surface and verify the equation

$$\tilde{b}_c = \frac{-\tilde{\sigma}}{z_c\int_1^s x^2 e^{-z_c\tilde{\Psi}^{(0)}(x)}\,dx} \quad (57)$$

which is obtained from the nondimensional form of eq 16, whereas the number of H^+ and OH^- ions must be equal due to the electroneutrality of the cell

$$\tilde{b}_{H^+}\int_1^s x^2 e^{-\tilde{\Psi}^{(0)}(x)}\,dx = \tilde{b}_{OH^-}\int_1^s x^2 e^{\tilde{\Psi}^{(0)}(x)}\,dx \quad (58)$$

We also need eq 52 to close the system of equations. The three boundary conditions for eq 56 are given by eq 51. In this case, an iterative method has to be used because of the unknown parameter $\tilde{b}_c$. The general procedure has been described in ref 11 and discussed in comparison with other approaches to solve the Poisson−Boltzmann equation. Once we have found the electric potential $\tilde{\Psi}^{(0)}(x)$, the parameters $\tilde{b}_{H^+}$, $\tilde{b}_{OH^-}$, and $\tilde{b}_c$ can be obtained from the system of eqs 52, 58, and

$$\tilde{\Psi}^{(0)\prime\prime}(s) = -z_c\tilde{b}_c - \tilde{b}_{H^+} + \tilde{b}_{OH^-} \quad (59)$$

and the equilibrium ionic concentrations by using eq 14.

In Figure 3 the effect on the electrophoretic mobility of considering an ionic species for the added counterions different from those of water dissociation is checked against volume fraction for different particle charges. The latter effect of decreasing mobility in the low particle concentration region when water dissociation ions were considered is now even larger if we compare between Figures 2 and 3. Qualitatively the role of K^+ and H^+ counterions is similar, but whereas the latter enters the water dissociation reaction, the former does not, what modifies considerably the counterions concentration inside the cell. In such conditions, the total number of counterions is larger for case b than for case a (the electroneutrality of the cell maintained in all cases). It was shown in a previous paper[11] that in case b the counterions screening effect is larger in comparison with that of case a, leading to lower surface potentials and consequently lower electrophoretic mobility values. In Figure 4 we compare between electrophoretic mobility predictions according to cases a and b. We can observe for the case of noncommon counterions (case b) a significant influence on decreasing mobility until higher volume fraction values in comparison with the case of common counterions (case a). In particular, for the largest particle charges the effect is remarkable for particle volume fractions less than $\approx 10^{-1}$. Likewise, it is important to point out the minor relevance of differentiating among common and noncommon added counterions when the particle charge is low.

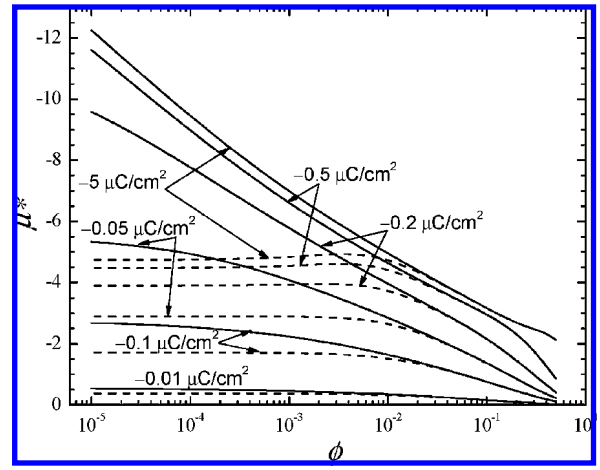

Figure 5. Nondimensional electrophoretic mobility against particle volume fraction for different surface charge densities. Solid lines: only added counterions H^+. Dashed lines, case a: added counterions H^+ with water dissociation and atmospheric contamination ions H^+, OH^-, HCO_3^-.

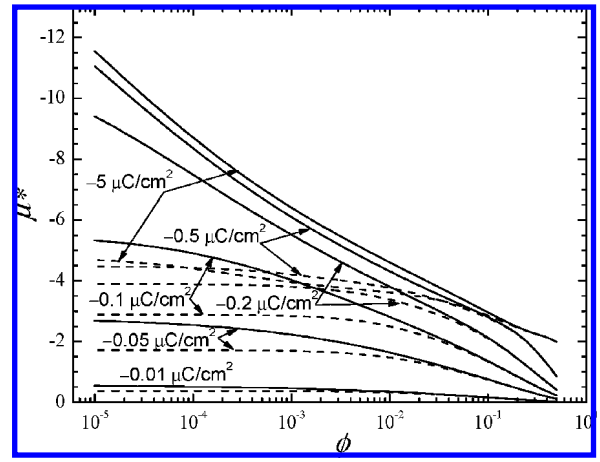

Figure 6. Nondimensional electrophoretic mobility against particle volume fraction for different surface charge densities. Solid lines: only added counterions K^+. Dashed lines, case b: added counterions K^+ with water dissociation and atmospheric contamination ions H^+, OH^-, HCO_3^-.

Electrophoretic Mobility: Added Counterions, Water Dissociation, and CO_2 Contamination. Let us consider now that, in addition to the added counterions and the H^+ and OH^- ions coming from water dissociation, there are also present ions stemming from the atmospheric CO_2 contamination in the liquid medium. This will always occur in aqueous suspensions in contact with the atmosphere: the CO_2 gas diffused into the suspension combines with water molecules to form carbonic acid H_2CO_3, and then, the following dissociation reactions take place:

$$\begin{aligned} CO_2 + H_2O &\rightleftarrows H_2CO_3 \\ H_2CO_3 &\rightleftarrows H^+ + HCO_3^- \\ HCO_3^- &\rightleftarrows H^+ + CO_3^{2-} \end{aligned} \quad (60)$$

with equilibrium dissociation constants $K_1 = 4.47 \times 10^{-7}$ mol/L and $K_2 = 4.67 \times 10^{-11}$ mol/L at room temperature (25 °C),

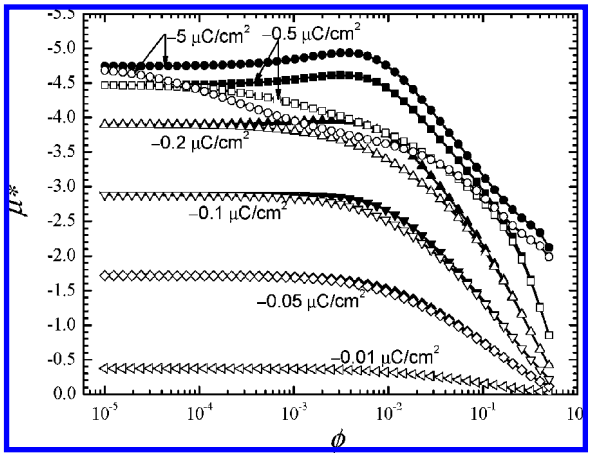

Figure 7. Nondimensional electrophoretic mobility against particle volume fraction for different surface charge densities and type of added counterions. Solid symbols, case a: added counterions H^+ with water dissociation and atmospheric contamination ions H^+, OH^-, HCO_3^-. Open symbols, case b: added counterions K^+ with water dissociation and atmospheric contamination ions H^+, OH^-, HCO_3^-.

respectively. The concentration of CO_2 molecules in water is completely determined from the solubility and the partial pressure of CO_2 in standard air. For a temperature of 25 °C and an atmospheric pressure of 101325 Pa, the concentration of carbonic acid is approximately $[H_2CO_3] = 2.0 \times 10^{-8}$ mol/L, and that of carbon dioxide is $[CO_2] = 1.08 \times 10^{-5}$ mol/L, depending its particular value on the local environmental conditions. The dissociation constants and this concentration are nondimensionalized as

$$\tilde{K}_1 = \frac{N_A e^2 a^2}{\varepsilon_{rs}\varepsilon_0 k_B T} K_1 \qquad \tilde{K}_2 = \frac{N_A e^2 a^2}{\varepsilon_{rs}\varepsilon_0 k_B T} K_2$$

$$\tilde{N}_{CO_2} = \frac{N_A e^2 a^2}{\varepsilon_{rs}\varepsilon_0 k_B T}[CO_2] \quad (61)$$

where all the values are taken in SI units. In ref 11 was pointed out the minor importance of the CO_3^{2-} ions because of the lower dissociation constant of its chemical dissociation reaction. Their role was therefore neglected in the study of the EDL because the obtained equilibrium electric potential profiles differed from the exact ones in less than 10^{-4} % in the worst of the cases studied. In what follows we will make use of this approximation.

We can distinguish between two cases: (a) when the added counterions are coincident with one of the ionic species in the system (H^+, OH^-, HCO_3^- ions) and (b) when they are of a different ionic species. In the a case the added counterions will enter in one of the equilibrium dissociation equations, whereas in the b case they do not.

Case a. According to ref 11, the nondimensional Poisson−Boltzmann equation is transformed to the form

$$\tilde{\Psi}^{(0)\prime\prime\prime}(x) + \frac{2}{x}\tilde{\Psi}^{(0)\prime\prime}(x) - \frac{2}{x^2}\tilde{\Psi}^{(0)\prime}(x) - \tilde{\Psi}^{(0)\prime}(x)\sqrt{\left(\tilde{\Psi}^{(0)\prime\prime}(x) + \frac{2}{x}\tilde{\Psi}^{(0)\prime}(x)\right)^2 + 4\tilde{E}_1} = 0 \quad (62)$$

where we have defined the constant $\tilde{E}_1 = \tilde{K}_w + \tilde{K}_1\tilde{N}_{CO_2}$, being the nondimensional constants expressed by eqs 53, 61 and

$$\frac{[H^+][HCO_3^-]}{[CO_2]} = K_1 \Rightarrow \frac{\tilde{b}_{H^+}\tilde{b}_{HCO_3^-}}{\tilde{N}_{CO_2}} = \tilde{K}_1 \quad (63)$$

and the ionic valences taken as $z_{H^+} = 1$, $z_{OH^-} = -1$, and $z_{HCO_3^-} = -1$. Equation 62 is solved numerically with the boundary conditions in eq 51 to give the equilibrium electric potential profile in one single step, avoiding any iterative procedure again. Once we have found the electric potential $\tilde{\Psi}^{(0)}(x)$, the parameters $\tilde{b}_{H^+}$, $\tilde{b}_{OH^-}$, and $\tilde{b}_{HCO_3^-}$ can be obtained from the system of eqs 52, 63 and

$$\tilde{\Psi}^{(0)\prime\prime}(s) = -\tilde{b}_{H^+} + \tilde{b}_{OH^-} + \tilde{b}_{HCO_3^-} \quad (64)$$

and the equilibrium ionic concentrations computed with the help of eq 14.

In Figure 5 we compare the electrophoretic mobility for pure salt-free suspensions with just their added counterions and for realistic ones with water dissociation plus CO_2 contamination ions. Again we can observe that for highly concentrated suspensions all the curves coincide, due to the predomination of added counterions over the water dissociation and CO_2 contamination ions. It was already shown[11] that the surface potential is seriously diminished reaching plateaus against volume fraction at the low concentrated particle region. This important effect extends from the very dilute limit to $\phi \approx 10^{-2}$ and provokes the mobility to attain nearly constant values in such low particle region. Due to that the H^+ counterions inside the cell arise from three different sources, (i) the charge process of the colloidal particle, (ii) the water dissociation equilibrium, and (iii) the proton dissociation from carbonic acid, we have a larger concentration of counterions in comparison with that of the pure salt-free case for given particle charge and volume fraction, which is responsible for the outstanding diminution of surface potential and electrophoretic mobility in the low volume fraction region.

Case b. We will adopt from the beginning the approximation made before. In this case, the nondimensional Poisson−Boltzmann equation is changed for numerical convenience to the form[11]

$$\tilde{\Psi}^{(0)\prime\prime\prime}(x) + \frac{2}{x}\tilde{\Psi}^{(0)\prime\prime}(x) - \frac{2}{x^2}\tilde{\Psi}^{(0)\prime}(x) - \tilde{\Psi}^{(0)\prime}(x) \times \left[\sqrt{\left(\tilde{\Psi}^{(0)\prime\prime}(x) + \frac{2}{x}\tilde{\Psi}^{(0)\prime}(x) + z_c\tilde{b}_c e^{-z_c\tilde{\Psi}^{(0)}(x)}\right)^2 + 4\tilde{E}_1} + z_c^2\tilde{b}_c e^{-z_c\tilde{\Psi}^{(0)}(x)}\right] = 0 \quad (65)$$

The three boundary conditions for this equation are given by eq 51. The system is solved again using the iterative procedure described in ref 11. Once we have found the electric potential $\tilde{\Psi}^{(0)}(x)$, the parameters $\tilde{b}_{H^+}$, $\tilde{b}_{OH^-}$, $\tilde{b}_{HCO_3^-}$, and $\tilde{b}_c$ can be obtained from the system of eqs 52, 57, 63, and

$$\tilde{\Psi}^{(0)\prime\prime}(s) = -z_c\tilde{b}_c - \tilde{b}_{H^+} + \tilde{b}_{OH^-} + \tilde{b}_{HCO_3^-} \quad (66)$$

the equilibrium ionic concentrations by means of eq 14.

Similarly to the studies addressed in a previous section concerning water dissociation effects with common and non-common added counterions, we now take into account the role of K^+ as added counterions when other noncommon ionic

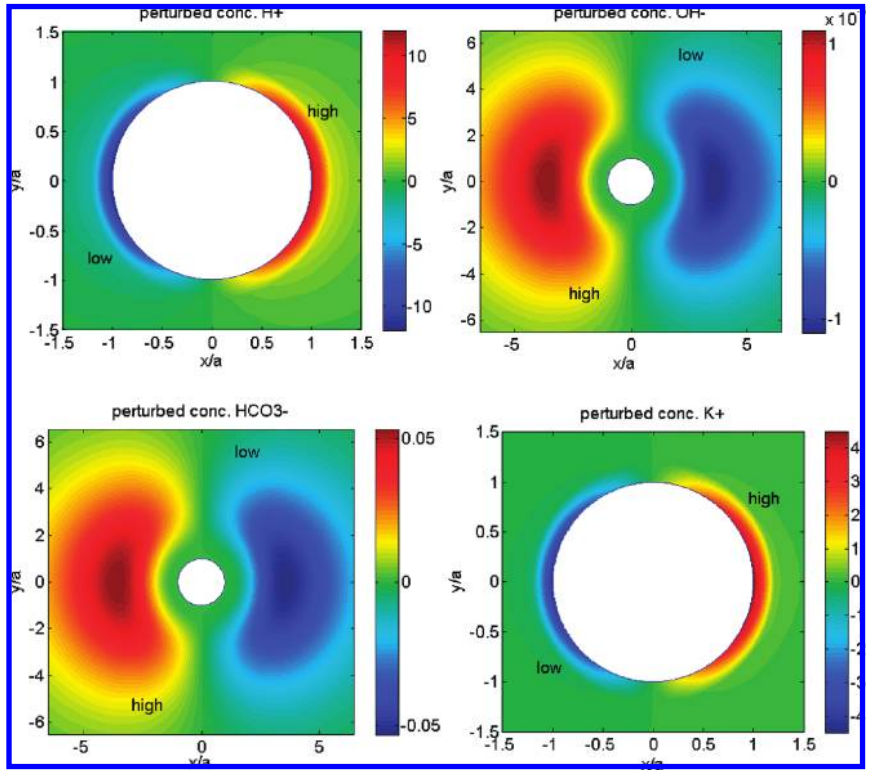

Figure 8. Two-dimensional plots of the nondimensional perturbations of ionic concentrations for a negatively charged particle in a realistic salt-free suspension at 25 °C corresponding to case b: added counterions K^+ with water dissociation and atmospheric contamination ions H^+, OH^-, HCO_3^-. $a = 100$ nm, $\phi = 0.0001$, $\sigma = -0.6$ μC/cm^2. In the figures the electric field points to the right.

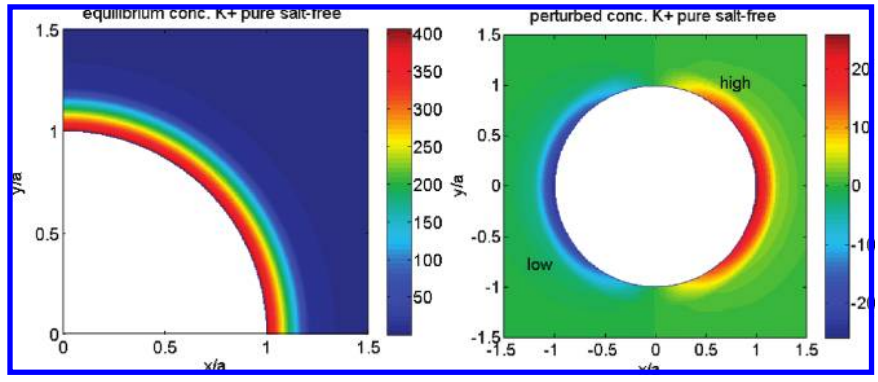

Figure 9. Two-dimensional plots of the equilibrium and perturbed nondimensional K^+ concentrations for a negatively charged particle in a pure salt-free suspension at 25 °C with just added counterions K^+. $a = 100$ nm, $\phi = 0.0001$, $\sigma = -0.6$ μC/cm^2. The electric field points to the right in the figures.

species are present due to water dissociation and CO_2 contamination effects (see Figure 6). As for common added counterions (case a) the effect is amazing for moderate to large particle charges, and even larger in the intermediate region of volume fractions as can be seen in Figure 7 where cases a and b are compared. In case b the dissociation reactions (see eq 60) cannot reduce the number of added counterions K^+ because these ions do not participate in them, whereas the H^+ counterions do (case a). The final result is an increasing shielding of the particle charge in case b in comparison with case a, with the exception of both the very dilute and the highly concentrated volume fraction regions. In the former the H^+ bulk counterions are mainly responsible for the observed behavior because of the low number of added counterions released by the particles at such low volume fractions. On the contrary, when the volume fraction is large enough, the added counterions from the particles dominate over water dissociation and CO_2 contamination ions leading to a perfect matching between realistic and pure salt-free results in Figures 6 and 7.

We can go a step further by exploring the perturbed ionic concentrations around a particle for different theoretical conditions when a dc electric field is applied. We have chosen for the study in Figure 8 the latter general case b (noncommon added counterions K^+ and water dissociation and CO_2 contamination) and in Figure 9 the pure salt-free case with just K^+ as added counterions, for theoretical conditions ($\phi = 0.0001$, $\sigma = -0.6$ μC/cm^2) where an important deviation of the standard (pure salt-free) electrophoretic mobility has been predicted (see Figure 6). Similar patterns for counterions H^+ and K^+ can be shown in Figure 8 (perhaps a large quantitative effect of H^+ over K^+ ions due to the larger diffusion coefficient of the former ones, see also ref 12 where a study of the influence that the diffusion coefficient of different counterions has on electrokinetic properties is made): a large excess in perturbed counterion

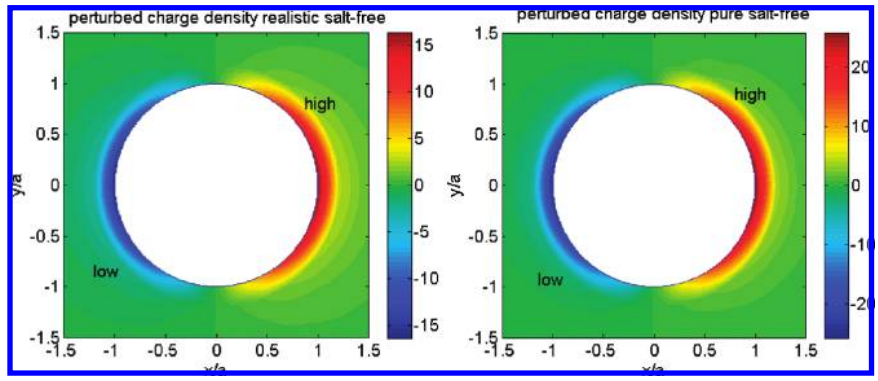

Figure 10. Two-dimensional plots of the perturbed nondimensional volume charge density for a negatively charged particle in realistic (Figure 8) and pure (Figure 9b) salt-free suspensions at 25 °C. The electric field points to the right in the figures.

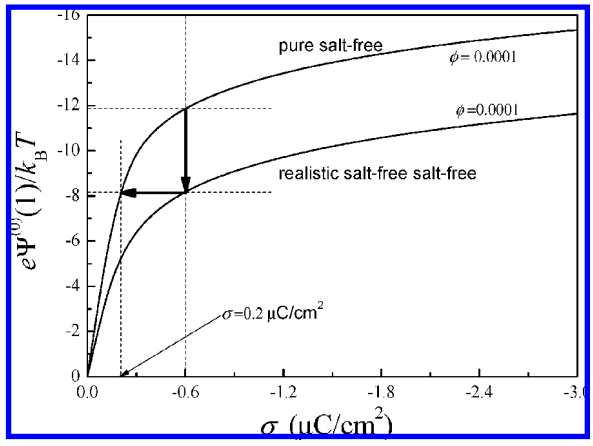

Figure 11. Nondimensional equilibrium surface potential against particle surface charge density for a negatively charged particle in realistic and pure salt-free suspensions at 25 °C, including the cases displayed in Figures 8 and 9.

concentration very close to the particle surface that quickly decays as we move away from it in the same direction of the field. At the other side of the particle the opposite situation takes place. For co-ions, a different trend is shown with maxima (excess at the left side of the particle) and minima (defect at the right side) perturbations in co-ion concentrations at certain distances from the particle surface, the role of HCO_3^- ions being relatively more important than the OH^- ions.

In Figure 9 we also display the equilibrium K^+ concentration (left panel) around a particle in a pure salt-free suspension to better appreciate and compare the magnitude of the perturbations (right panel) in counterion concentration due to the electric field. The electric polarization of the double layer greatly influences the final electrokinetic behavior of the particles. A relationship between the electrophoretic mobility and the induced dipole moment of the particles is then expected, but due to the mathematical complexity no general analytical relationship is attainable.[49] However, for salt suspensions it is known that in stationary conditions with large particle surface conductance, tangential ionic flows caused by the surface conductivity are mainly responsible for induced charges. This contribution generates a dipole moment pointing in the direction of the electric field. On the contrary, for very low particle surface conductance the field-induced ionic charge is mainly due to normal fluxes to the surface, generating a dipole moment in the opposite direction of the electric field.[49] Simultaneously, diffusion currents tend to diminish the accumulation (depletion) of ions at both sides of the particle due to the field, decreasing the magnitude of the induced dipole moment. In the first case of large surface conductance, the larger the magnitude of the induced dipole moment, the larger its capacity of breaking the electrophoretic motion[49] through electrophoretic relaxation forces. These are associated with the deviation of the double layer from spherical symmetry and surface conductivity due to the excess ions in it, but this is not the unique electric contribution in breaking the particle motion. Ions in the double layer transfer part of the electrostatic force the electric field exerts on them to the particle surface through viscous stress. This part of the force that is applied to the particle body is called electrophoretic retardation force. Fluxes of counterions and co-ions driven by the electric field in the realistic case, or just counterions in the pure salt-free one, will contribute to this force. The larger ionic strength for the former case leads to an expected larger electrophoretic retardation in comparison with pure salt-free conditions.

Turning back to the cases studied in Figures 8 and 9, it can be inferred that the positive electric dipole induced by the field seems to be less significant for the realistic case depicted in Figure 8 than that in Figure 9, in spite of the larger surface conductance for the realistic case due to the increasing number of ions of different ionic species in the double layer. This affirmation is supported by the results in Figure 10 showing the stationary distributions around a particle of the perturbed volume charge density $\delta\rho = \sum_{i=1}^{n} z_i e \delta n_i$ for the two cases, which can be used to compute the induced dipole moments by means of the equation

$$\delta\vec{\mathbf{p}} = \int_V \vec{\mathbf{r}}\,\delta\rho\,dV \tag{67}$$

that, in nondimensional units, becomes

$$\delta\vec{\mathbf{p}} = \frac{\delta\vec{\mathbf{p}}}{4\pi a^3 E \varepsilon_{rs}\varepsilon_0} = \frac{1}{3}\sum_{i=1}^{n} z_i^2 \tilde{b}_i \int_1^s x^3 \exp[-z_i\tilde{\Psi}^{(0)}(x)][\tilde{Y}(x) - \tilde{\phi}_i(x)]\,dx\,\tilde{\mathbf{k}} \tag{68}$$

$\hat{\mathbf{k}}$ being the direction of the electric field. For the cases displayed in Figure 10, the induced dipole moments in nondimensional units turn out to be 40.61 and 100.21, for realistic and pure salt-free conditions, respectively. Therefore, it can be concluded that it is the larger electrophoretic retardation effect in realistic conditions that is the one responsible for the lower mobilities attained in such cases. This is probably what happens because the larger concentration of ions around the particle for realistic situations not only should lead to larger electrophoretic retarda-

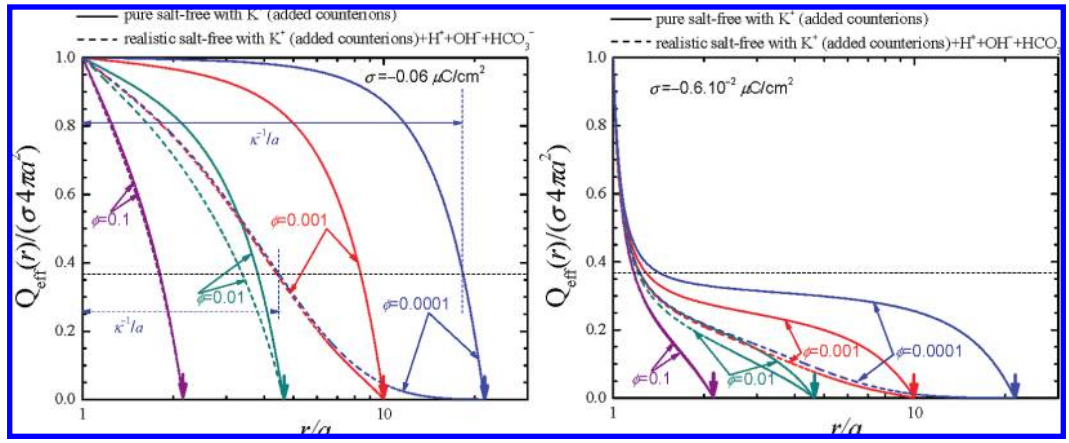

Figure 12. Effective particle charge at different radial distances inside a unit cell, for two different particle surface charge densities. The vertical arrows at the bottom indicate the limit of the outer surface of the cell for every particle volume fraction displayed. The effective particle charges are zero in the latter points due to the electroneutrality of the cells. $a = 100$ nm.

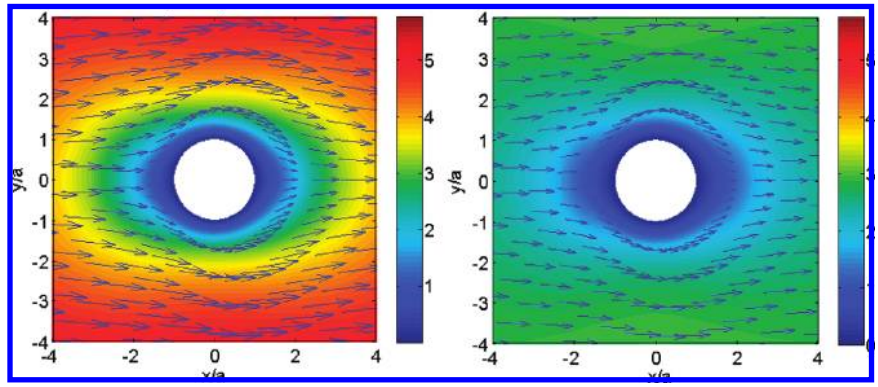

Figure 13. Two-dimensional plots of the nondimensional fluid velocity field around a negatively charged particle in a pure salt-free suspension with just added counterions K^+ (left) and in a realistic salt-free suspension (right) corresponding to case b: added counterions K^+ with water dissociation and atmospheric contamination ions H^+, OH^-, HCO_3^-, at 25 °C. $a = 100$ nm, $\phi = 0.0001$, $\sigma = -0.6$ μC/cm^2. The reference system is fixed at the center of the particle. In the figures the electric field points to the right.

tion effects but also to enhanced charge screening effects and, consequently, to lower surface potentials in such conditions. This conclusion has been already reported when comparing the pure salt-free surface potential with that according to the realistic case[11] for different theoretical conditions. Thus, in Figure 11 we can see that for $\phi = 0.0001$ and $\sigma = -0.6$ μC/cm^2 the surface potential decreases from nearly -12 (pure salt-free) to -8 (realistic salt-free) in standard nondimensional units. One might be tempted to consider that a realistic salt-free suspension at a given particle volume fraction behaves as an equivalent "pure salt-free" one with a lower particle surface charge. For the case in study, it is shown in Figure 11 that an "equivalent pure salt-free surface charge" of -0.2 μC/cm^2 would correspond to the realistic case of -0.6 μC/cm^2.

But in the presence of an electric field, this simplified image is not consistent with the electrophoretic mobility predictions in Figure 6, where for $\sigma = -0.2$ μC/cm^2 the pure salt-free mobility turns out to be -7.5 instead of -4.5, the latter being the value for the realistic case with $\sigma = -0.6$ μC/cm^2. The augmented concentration of counterions in the realistic case, that explains the mobility decrease due to the enhanced retardation force, also makes a better screening of the particle charge, causing and important diminution of the surface potential. This effect more than compensates the mobility increase that one might expect when the magnitude of the positive induced dipole moment decreases, in accordance with Figure 10 and results by eq 68.

From another point of view, this remarkable decreasing effect of the surface potential in real situations can be understood by comparing the net or effective particle charge for realistic and pure salt-free conditions as we move away from the particle surface. This can be done by integrating the volume charge density in the liquid medium from the particle surface to an arbitrary distance inside the cell. It is easy to demonstrate that this net or effective charge $Q_{\text{eff}}(r)$ at a given radial distance r from the center of the particle is given by

$$\frac{Q_{\text{eff}}(r)}{\sigma 4\pi a^2} = 1 + \frac{1}{\tilde{\sigma}}[(\tilde{b}_{H^+} + \tilde{b}_{K^+})\int_1^x \exp[-\tilde{\Psi}^{(0)}(x)]x^2\,dx - (\tilde{b}_{OH^-} + \tilde{b}_{HCO_3^-})\int_1^x \exp[\tilde{\Psi}^{(0)}(x)]x^2\,dx] \quad (69)$$

for a realistic salt-free suspension with K^+ as added counterions, and

$$\frac{Q_{\text{eff}}(r)}{\sigma 4\pi a^2} = 1 + \frac{1}{\tilde{\sigma}}[\tilde{b}_{K^+}\int_1^x \exp[-\tilde{\Psi}^{(0)}(x)]x^2\,dx] \quad (70)$$

for a pure salt-free suspension with K^+ as added counterions.

We can also define a more correct κa parameter representing the inverse of the nondimensional distance from the particle surface to which the effective particle charge equals the particle

charge divided by e, i.e., $\kappa a = \{[(a + \kappa^{-1}) - a]/a\}^{-1}$, with $a + \kappa^{-1}$ the corresponding distance from the center of the particle to which the condition expressed by

$$\frac{Q_{\text{eff}}(a + \kappa^{-1})}{\sigma 4\pi a^2} = \frac{1}{e} \tag{71}$$

fulfills.

The latter is one of the many possible definitions trying to give us an idea of the spread of ionic concentration profiles in the cell. In that sense, it may help to better characterize the ionic screening effect when comparing between different salt-free conditions. In Figure 12 we display the effective particle charge calculated for different situations of surface charge and volume fraction for realistic and pure salt-free suspensions. A very clear correlation between these curves and the mobility curves in Figure 6 can be observed. The enhanced charge screening effect due to water dissociation and CO_2 contamination in comparison with those of the pure salt-free cases, which has led to lower surface potentials in such conditions, agrees well with the important decrease of the mobility observed in realistic situations. The cross of the horizontal dashed lines to the curves in Figure 12 shows for every case the position where the effective charge is equal to the particle charge reduced by a factor e. As an example, for the case of lowest charge and volume fraction studied (Figure 12, left panel), we can numerically calculate with the help of eqs 69−71 the κa parameters: 0.058 and 0.29, corresponding to the pure and realistic salt-free cases, respectively. This supposes that the "width of the double layer" for the pure salt-free case is (in particle radius units) approximately equal to 17.29, whereas for the realistic case it is 3.47 (both indicated by horizontal arrows in Figure 12), 20.5 being the scaled distance between the surface of the particle and the outer surface of the cell. The above-mentioned larger screening effect expected in realistic salt-free cases in comparison with pure salt-free ones is thus well represented by the proposed κa parameter.

Alternatively, the decrease in the electrophoretic mobility for the particular case studied in Figures 8−10 can be numerically confirmed in Figure 13 by just computing the fluid velocity field around a particle for the pure and realistic salt-free conditions of Figures 8 and 9 (right panel). From the reference system linked to the center of the particle, the fluid velocity attains larger velocities for the pure salt-free case, which is seen as a larger particle velocity from the laboratory reference system.

Summarizing, it has been shown that in many cases the theoretical electrophoretic mobility changes dramatically when water dissociation and CO_2 contamination are taking into account. It would be very convenient to test these predictions with appropriate experiments due to the magnitude of the corrections involved, and we encourage experimentalists to face this issue to properly quantify the role of these effects.

Conclusions

On the basis of a "realistic" description of the electric double layer for salt-free concentrated suspensions[11] which takes into account effects as water dissociation and CO_2 contamination in the suspensions, we have studied their influence on the dc electrophoretic mobility of a spherical particle. The numerical results have clearly shown quite important changes in the theoretical electrophoretic mobility predictions, as compared to those in pure salt-free systems, even when solely water dissociation effects are incorporated to the standard salt-free theory. These changes are larger the lower the particle volume fraction but still more striking if in addition to water dissociation we allow for atmospheric CO_2 contamination by assuming that the suspensions could have been exposed to air during the preparation or during the experimental measurement procedure. The results also show that it is important to distinguish whether the added counterions coincide or not with one of the ionic species arising from the dissociation of water and carbonic acid. To properly test the model new experiments have to be performed to measure the electrophoretic mobility before and after the samples have been exposed to the atmosphere. That would let us control and quantify the CO_2 influence on the mobility values. We think that the present work establishes the starting point for the development of future theories about the electrokinetics, rheology, and phase behavior of realistic salt-free concentrated suspensions.

Acknowledgment. Financial support for this work by Ministerio de Educación y Ciencia, Spain, project FIS2007-62737, and Junta de Andalucía, Spain, project P08-FQM-03779 (co-financed with FEDER funds by the European Union), is gratefully acknowledged.

References and Notes

(1) Medebach, M.; Palberg, T. *J. Chem. Phys.* **2003**, *119*, 3360.
(2) Medebach, M.; Palberg, T. *Colloids Surf., A* **2003**, *222*, 175.
(3) Chiang, C. P.; Lee, E.; He, Y. Y.; Hsu, J. P. *J. Phys. Chem. B* **2006**, *110*, 1490.
(4) Ohshima, H. *J. Colloid Interface Sci.* **2002**, *247*, 18.
(5) Ohshima, H. *J. Colloid Interface Sci.* **2002**, *248*, 499.
(6) Ohshima, H. *J. Colloid Interface Sci.* **2003**, *262*, 294.
(7) Ohshima, H. *J. Colloid Interface Sci.* **2003**, *265*, 422.
(8) Ruiz-Reina, E.; Carrique, F. *J. Phys. Chem. C* **2007**, *111*, 141.
(9) Carrique, F.; Ruiz-Reina, E.; Arroyo, F. J.; Delgado, A. V. *J. Phys. Chem. B* **2006**, *110*, 18313.
(10) Ohshima, H. *Theory of Colloid and Interfacial Electric Phenomena*; Academic Press: Amsterdam, The Netherlands, 2006.
(11) Ruiz-Reina, E.; Carrique, F. *J. Phys. Chem. B* **2008**, *112*, 11960.
(12) Carrique, F.; Ruiz-Reina, E.; Arroyo, F. J.; Jimenez, M. L.; Delgado, A. V. *Langmuir* **2008**, *24*, 2395.
(13) Carrique, F.; Ruiz-Reina, E.; Arroyo, F. J.; Jimenez, M. L.; Delgado, A. V. *Langmuir* **2008**, *24*, 11544.
(14) Alexander, S. *J. Chem. Phys.* **1984**, *80*, 5776.
(15) Trizac, E.; Belloni, L.; Dobnikar, J.; von Grunberg, H. H.; Castaneda-Priego, R. *Phys. Rev. E* **2007**, *75*, 011401.
(16) Pianegonda, S.; Trizac, E.; Levin, Y. *J. Chem. Phys.* **2007**, *126*, 014702.
(17) von Grunberg, H. H. *J. Colloid Interface Sci.* **1999**, *219*, 339.
(18) Belloni, L. *Colloids Surf., A* **1998**, *140*, 227.
(19) Robbins, M. O.; Kremer, K.; Grest, G. S. *J. Chem. Phys.* **1988**, *88*, 3286.
(20) Palberg, T.; Monch, W.; Bitzer, F.; Leiderer, P.; Belloni, L.; Bellini, T.; Piazza, R. *Helv. Phys. Acta* **1994**, *67*, 225.
(21) Russel, W. B.; Saville, D. A.; Schowalter, W. R. *Colloidal Dispersions*; Cambrige University Press: Cambridge, U.K., 1989.
(22) Levine, S.; Neale, G. H. *J. Colloid Interface Sci.* **1974**, *47*, 520.
(23) Ohshima, H. *J. Colloid Interface Sci.* **1999**, *212*, 443.
(24) Lee, E.; Chih, M. H.; Hsu, J. P. *J. Phys. Chem. B* **2001**, *105*, 747.
(25) Carrique, F.; Arroyo, F. J.; Delgado, A. V. *J. Colloid Interface Sci.* **2002**, *252*, 126.
(26) Levine, S.; Neale, G. H.; Epstein, N. *J. Colloid Interface Sci.* **1976**, *57*, 424.
(27) Ohshima, H. *J. Colloid Interface Sci.* **1998**, *208*, 295.
(28) Ohshima, H. *J. Colloid Interface Sci.* **1997**, *195*, 137.
(29) Lee, E.; Yen, F. Y.; Hsu, J. P. *J. Phys. Chem. B* **2001**, *105*, 7239.
(30) Hsu, J. P.; Lee, E.; Yen, F. Y. *J. Phys. Chem. B* **2002**, *106*, 4789.
(31) Carrique, F.; Arroyo, F. J.; Jiménez, M. L.; Delgado, A. V. *J. Chem. Phys.* **2003**, *118*, 1945.
(32) Ruiz-Reina, E.; Carrique, F.; Rubio-Hernández, F. J.; Gómez-Merino, A. I.; García-Sánchez, P. *J. Phys. Chem. B* **2003**, *107*, 9528.
(33) Ruiz-Reina, E.; Garcia-Sanchez, P.; Carrique, F. *J. Phys. Chem. B* **2005**, *109*, 5289.
(34) Carrique, F.; Garcia-Sanchez, P.; Ruiz-Reina, E. *J. Phys. Chem. B* **2005**, *109*, 24369.
(35) Ohshima, H.; Dukhin, A. S. *J. Colloid Interface Sci.* **1999**, *212*, 449.

(36) Dukhin, A. S.; Ohshima, H.; Shilov, V. N.; Goetz, P. J. *Langmuir* **1999**, *15*, 3445.
(37) Zholkovskij, E. K.; Masliyah, J. H.; Shilov, V. N.; Bhattacharjee, S. *Adv. Colloid Interface Sci.* **2007**, *134*−*135*, 279.
(38) Happel, J. *J. Appl. Phys.* **1957**, *28*, 1288.
(39) Kuwabara, S. *J. Phys. Soc. Jpn.* **1959**, *14*, 527.
(40) O'Brien, R. W.; White, L. R. *J. Chem. Soc., Faraday Trans. 2* **1978**, *74*, 1607.
(41) Ohshima, H.; Healy, T. W.; White, L. R. *J. Chem. Soc., Faraday Trans. 2* **1983**, *79*, 1613.
(42) DeLacey, E. H. B.; White, L. R. *J. Chem. Soc., Faraday Trans. 2* **1981**, *77*, 2007.
(43) Ohshima, H. *J. Colloid Interface Sci.* **1997**, *188*, 481.
(44) Shilov, V. N.; Zharkikh, N. I.; Borkovskaya, Y. B. *Colloid J.* **1981**, *43*, 434.
(45) Lee, E.; Chu, J. W.; Hsu, J. *J. Chem. Phys.* **1999**, *110*, 11643.
(46) Carrique, F.; Arroyo, F. J.; Delgado, A. V. *J. Colloid Interface Sci.* **2001**, *243*, 351.
(47) Dukhin, A. S.; Shilov, V. N.; Borkovskaya, Y. B. *Langmuir* **1999**, *15*, 3452.
(48) Shampine, L. F.; Kierzenka, J. Solving boundary value problems for ordinary differential equations in MATLAB with bvp4c; The MathWorks, Inc., 2000; available at http://www.mathworks.com/bvp_tutorial.
(49) Shilov, V. N.; Delgado, A. V.; González-Caballero, F.; Horno, J.; López-García, J. J.; Grosse, C. *J. Colloid Interface Sci.* **2000**, *232*, 141.

JP9015905